DESIGN AND CONSTRUCTION OF A TORSION FATIGUE MACHINE: TORSION FATIGUE TESTS ON TWO INDUSTRIAL ALUMINUM ALLOYS

Jorge L. AVILA AMBRIZ[1], Gonzalo M. DOMINGUEZ ALMARAZ[2], Julio C. VERDUZCO JUAREZ[3], Erasmo CORREA GOMEZ[4], Ishvari F. ZUÑIGA TELLO[5]

Most of fatigue machines used for industrial or laboratory applications are limited to perform a single fatigue test and its components are commonly servo-hydraulic or pneumatic actuators of high torque capability, leading to high costs. In the present paper is shown a torsion fatigue machine which works from 0.3 to 10 N-m of torque and it is used to investigate the fatigue torsion endurance for industrial materials, such as: steels, aluminum alloys, cast irons and polymers. This machine employs servomotors mounted with a linear motion mechanism to develop fatigue tests under torsion. The control and programming of angular motion is carried out by the freeware "Robotis" software, allowing an easy control for angular rotation. In this work is presented the general methodology for the setup of torsion tests: calibration of rotation motion, numerical simulation and the experimental results of torsion tests. Furthermore, this machine allows working at different load ratios R by applying an initial static angle before the initiation of torsion testing.

Keywords: Torsion fatigue machine, Torsion energy evaluation, Design – automatization, Torsion endurance, Fracture surfaces.

1. Introduction

The fatigue behavior of industrial materials is of principal interest to warrant the safety of the component in service; particularly under oscillating mechanical loads leading to mechanical fatigue [1-4]. In this matter, it's important to evaluate the experimental fatigue endurance of engineering materials due to the fact that theoretical equations do not always fit the real fatigue behavior [5, 6].

[1] Faculty of Mechanical Engineering, University of Michoacan (UMSNH), 58000, Mexico, Mexico, email: joavam@hotmail.com
[2] Faculty of Mechanical Engineering, University of Michoacan (UMSNH), 58000, Mexico, Mexico, email: dalmaraz@umich.mx
[3] Faculty of Mechanical Engineering, University of Michoacan (UMSNH), 58000, Mexico, Mexico, email: julio_glenn83@hotmail.com
[4] Faculty of Mechanical Engineering, University of Michoacan (UMSNH), 58000, Mexico, Mexico, email: etrasmo@gmail.com
[5] Faculty of Mechanical Engineering, University of Michoacan (UMSNH), 58000, Mexico, Mexico, email: isfernanda@hotmail.com

Then, it results necessary to carry out mechanical fatigue tests in different modalities and on a wide variety of materials to investigate the principal causes of failure in engineering components subjected to uniaxial and multiaxial loading [7-9]. Several authors have designed and constructed their own machines for specific applications [10-12]. In regard the torsion fatigue machines, the first prototype was developed in the nineteen century [13], in this machine load was induced by mechanical deflexion and inertia forces. The systematic studies on torsion fatigue have been carried out in the second half of the twenty century on aluminum alloys [14]; whereas most recent developments are oriented to the torsion fatigue machines controlled by a servo-actuator [15], or the use of a resonance system to induce failure by torsion [16]. This developed machine is oriented to perform torsion tests under displacement-controlled mode. The description of the present fatigue machine includes the process to carry out torsion fatigue tests: the first step is the selection of testing specimen and the definition of its profile by Autocad software, followed by the machining process of the specimen using a CNC station. At the same time, it is necessary to carry out numerical simulations to determine the maximum shear stress at the neck section of testing specimen, induced by a torsion applied loading.

This paper contains the following sections: section 2 is related to materials and methods, as well as the general aspects of testing specimen; the numerical analysis to determine the required load for torsion test is described in section 3, as well as the evaluation of the theoretical elastic energy accumulated by the torsion loading; whereas the design and general description of the torsion testing machine is presented in section 4. Finally, section 5 details the experimental results accompanied with discussion.

2. Materials and Methods

2.1. Specimen's geometry

The specimen used in this machine corresponds to the hourglass shape profile due its capability to induce a high stress concentration at the neck section under torsion tests [17]. The minimum diameter has been chosen close to 3 mm, Fig. 1a; this value was fixed to induce a maximum shear stress for each testing material and each applied load level. The used stress levels have been: 90, 80, 70, and 60% regarding the shear stress of the tested 6063.T5 aluminum alloy. It is important to notice that there is no available international standardization nowadays for torsion fatigue specimens; the norm ASTM-A938-07(2013) concerns the uniform section wire under torsion tests [18].

The dimensions of aluminum specimens meant for the present torsion machine have initially presented an industrial profile as-received, that is: hot-pressed rod of ¼” of diameter. This dimension is commonly available for a wide

variety of metallic alloys and industrial polymers. The Fig. 1a shows the dimensions (mm), of the hourglass shape torsion specimen.

2.2. Machining process

In order to avoid significant variations on the dimensions of testing specimens, the machining process was implemented in a CNC turning station under controlled machining parameters leading to diminish the high variation on the surface roughness: the roughness parameter Ra (arithmetic average of absolute values) was close to 10 μm for all testing specimens. As previously mentioned, specimen profiles for torsion fatigue testing are not standardized; some authors have used different profiles and dimensions [19-22]; nevertheless, it is observed that the hourglass shape profile is a constant for the torsion fatigue tests. Fig. 1b illustrates the as-received bar and the machined symmetric hourglass shape specimens used in this torsion fatigue machine.

3. Numerical analysis of shear stress distribution and elastic energy determination under torsion loading

3.1 Testing specimen

The general conditions for the torsion testing specimen are as follows: the bottom end of specimen was clamped and the torsion angle is applied at the top end, as shown in Fig. 2a. Parallel to the specimen's machining process, numerical simulations were carried out to determine the relationship between: the torque or applied rotational angle on the specimen and the induced shear stress at the neck section, as illustrated in Fig. 2b.

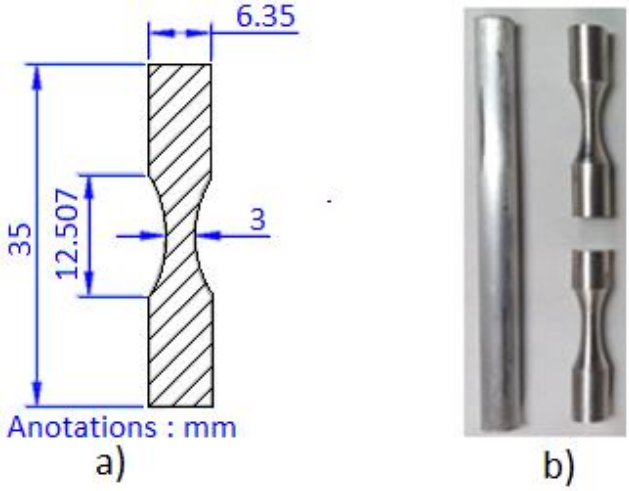

Fig. 1 a) Torsion specimen dimensions (mm). b) Commercial bar and machined torsion fatigue specimens

With the aid of numerical simulations, it's possible to predict the shear stress induced at the neck section when applying a torsion angle. The Fig. 2a shows the constraints and dimensions of torsion testing specimen; whereas Fig. 2b presents the shear stress distribution on the X-Y plane under torsion loading of one degree on the aluminum alloy 6061-T6. The highest shear stress observed under this torsion load has been 43.8 MPa, located at the neck section of testing specimen.

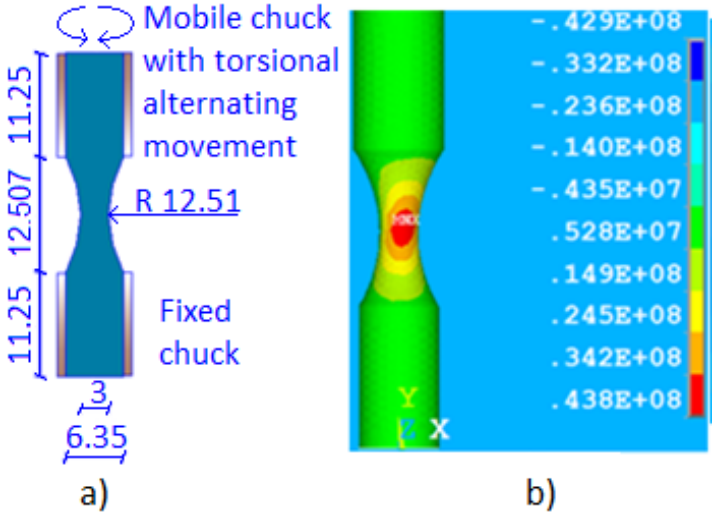

Fig. 2 a) Dimensions (mm) of testing specimen and testing constrains, b) Shear stress distribution in Pascals on the X-Y plane, for one degree of the torsion applied angle.

Concerning the loading regime, the load ratio R = 0 was imposed from a non-stressed initial position 0° to the maximum stress, following the clock wise direction, as shown in Fig. 3a. The load ratio R=-1 was implemented as show in Fig. 3b: from the no loaded position (0° on Fig. 3b), the specimen is mounted and a starting torsion angle is imposed in the clockwise direction; then, it oscillates from the last position between the maximum and minimum angle in alternating direction (clockwise direction and counter-clockwise direction, as illustrated in the same figure).

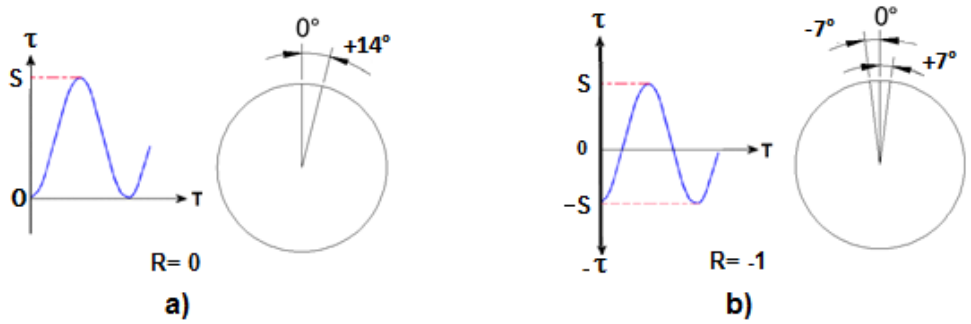

Fig. 3 Torsion displacements for the two load ratios: a) Load ratio R = 0, b) Full reverse loading R = -1.

3.2. Elastic energy accumulated by torsion loading.

Elastic energy is accumulated under torsion loading and is the product of applied torque T and the torsion angle θ:

$$E = \frac{1}{2} T\theta \tag{1}$$

In Fig. 4a is shown the free-body diagram for the section of torsion displacement on testing specimen; this section corresponds to the variable diameter along the specimen. The radius along this section is a quadratic function of the coordinate x:

$$R(x) = a + b\,x^2 \tag{2}$$

For x = 0, the radius is R = 0.0015 m, whereas for x = ± 0.006254 m, the radius is R = 0.003175 m; then, a = 0.0015 and b = 42.825. The polar moment of inertia for the section A-B is written as:

$$J_{AB} = \frac{\pi}{2} R^4 = \frac{\pi}{2} (0.0015 + 42.825\,x^2)^4 \tag{3}$$

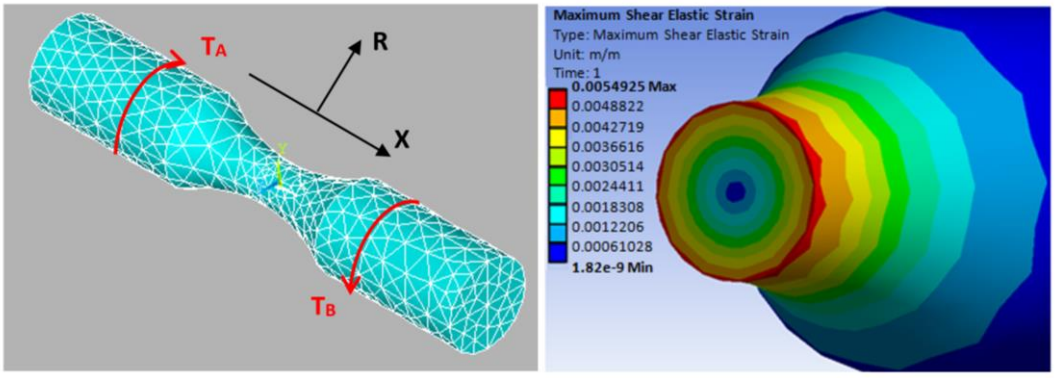

Fig. 4 a) Free body diagram for the torsion specimen, b) Shear strain corresponding to 0.64 Nm of applied torque

And the relative differential rotation at section A with respect to the section at B is:

$$\left(\frac{\mathbf{D\theta}}{\mathbf{dx}}\right)_{\mathbf{AB}} = \frac{\mathbf{T_{AB}}}{\mathbf{G_{AB}J_{AB}}} = \frac{\mathbf{T_{AB}}}{\mathbf{G_{AB}\frac{\pi}{2}\left(0.0015+42.825\,x^2\right)^4}} \tag{4}$$

Where G_{AB} is the shear modulus for the testing material (26 GPa for the aluminum alloy 6061-T6). Integrating the last equation gives:

$$\int_{\Theta_B}^{\theta_A} \mathbf{d\theta} = \int_{-0.006254}^{0.006254} \frac{\mathbf{T_{AB}}}{\mathbf{G_{AB}\frac{\pi}{2}\left(0.0015+42.825\,x^2\right)^4}}\,\mathbf{dx} \tag{5}$$

With the result for the torsion angle on A:

$$\theta_A = \frac{2T_{AB}}{G_{AB}\pi}\left[\frac{2.16212\,10^6x^5 + 201.949x^3 + 0.00583565x}{(x^2 + 0.0000350263)^3} + 3.65327\;10^8\,tan^{-1}(168.967x)\right]_{-0.006254}^{0.006254} \tag{6}$$

And in substituting the limits of integration, it results:

$$\theta = \frac{2T_{AB}}{G_{AB}\pi}\,(1.117037\;x\;10^9) \tag{7}$$

Values for θ are in radians, T_{AB} in Nm and G_{AB} in Pascals. An applied torque T_{AB} = 0.64 Nm on the aluminum alloy 6061-T6 specimen induces a torsion angle θ = 0.0175 rad ≈1 degree. Under the last conditions of loading and testing material, the elastic energy accumulated along the variable diameter section of Fig. 4a is obtained by:

$$E = \frac{1}{2}T\theta = \frac{1}{2}\,0.64\,(0.0175) = 0.0056\,J \tag{8}$$

On Fig. 4b is presented the shear elastic strain along the variable radius section: the maximum values are located at the surface and at the neck section of specimen. These values corresponding to the aluminum alloy 6061-T6 with an applied torque T_{AB} = 0.64 N-m.

A general expression for the differential torsion angle between A and B in function of geometrical properties of testing specimen (quadratic profile, equation 2) is as follows:

$$\left(\frac{\mathbf{D\theta}}{\mathbf{dx}}\right)_{\mathbf{AB}} = \frac{\mathbf{T_{AB}}}{\mathbf{G_{AB}J_{AB}}} = \frac{\mathbf{T_{AB}}}{\mathbf{G_{AB}\frac{\pi}{2}\left(a+b\,x^2\right)^4}} \tag{9}$$

Integrating along the variable radius section, Fig. 4a, the resulting expression is:

$$\int_{\Theta_B}^{\theta_A} \mathbf{d\theta} = \int_{-c}^{c} \frac{T_{AB}}{G_{AB}\frac{\pi}{2}(a+b\,x^2)^4}\,\mathbf{dx} \tag{10}$$

With the result after integration:

$$\theta_A = \frac{2T_{AB}}{G_{AB}\pi}\left[\frac{5tan^{-1}\left(\frac{\sqrt{b}\,x}{\sqrt{a}}\right)}{16a^{7/2}\sqrt{b}} + \frac{5x}{16a^3\,(a+bx^2)} + \frac{5x}{24a^2\,(a+bx^2)^2} + + \frac{x}{6a\,(a+bx^2)^3}\right]_{-c}^{c} \tag{11}$$

The integration limits [-*c*, *c*] correspond to a third geometrical property of testing specimen: the length of the variable radius section. Concerning the constant *b* in equation 2, its value is obtained by:

$$b = (R(c) - a)/c^2 \tag{12}$$

On Fig. 5 are plotted the evolution of the torsion angle θ, against the three geometrical dimensions of testing specimen: *a*, *b* and *c*, for constant values of T_{AB} and G_{AB}. The radius at the neck section of specimen a, seems to be a critical parameter for the increase of the rotation angle: the reduction of a induces an exponential growth to the fourth power on θ. The reduction on parameter *b* induces a moderate increase on the torsion angle θ; whereas the torsion angle increases with the geometrical dimension *c*, from 0 to an asymptotical value.

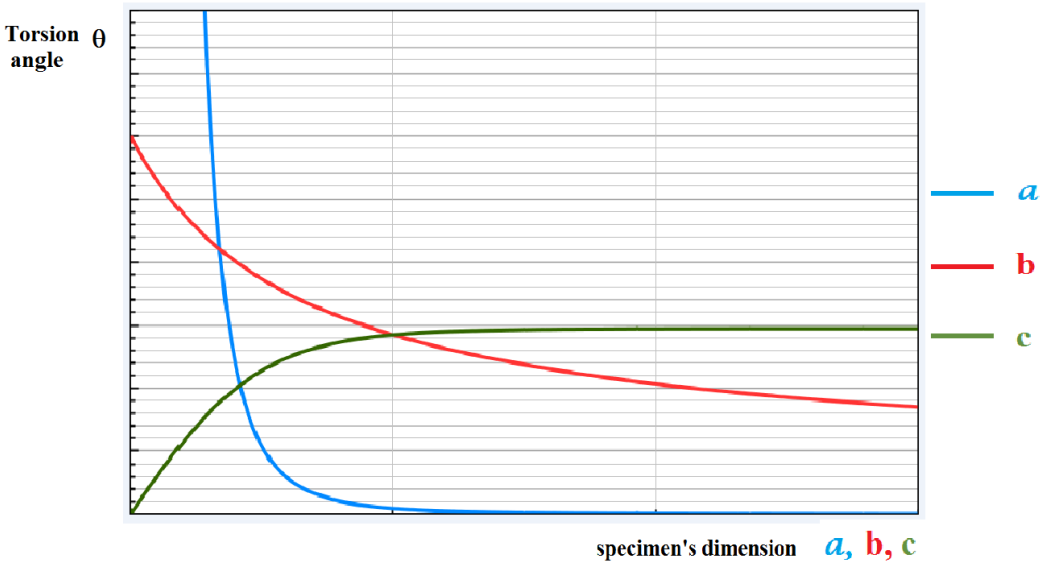

Fig. 5 Qualitative evolution of torsion angle θ with the specimen's geometrical dimensions: *a*, *b*, *c*

4. Design and description of the torsion fatigue machine.

In Fig. 6 is shown the fatigue machine designed for torsion fatigue tests. A DYNAMIXEL MX-106R servomotor is used to communicate rotating motion to the vertical or principal axis through a chain and gears; whereas a linear actuator induces deflection to achieve the bending modality. Both actuators work at 12 VDC and are controlled by the interface of a program developed with the "Robotis" platform, allowing communicating rotating motion with 0.1 degrees of precision. In this way, the vertical axis connects with testing specimen through a free torsion chuck and the specimen's bottom end is clamped by a second fixed chuck.

The Fig. 7a shows the final assembled machine and components; the manufacture process is described in other published work [23]. Two aluminum plates support the linear and rotary actuator, whereas the four columns of "celoron" material isolate the upper and lower aluminum plates of the machine. The Fig. 7b shows in detail the chucks and torsion specimen; it is noticeable that the fixed or inferior chuck is clamped to a steel plate which is separated by 4 mm from the lower aluminum plate: when the specimen is broken, its two broken parts are separated and the fixed chuck drops (4 mm) together with the steel plate. This particularity allows separating the two broken parts of specimen when fracture occurs, avoiding to damage the fracture surfaces due to friction.

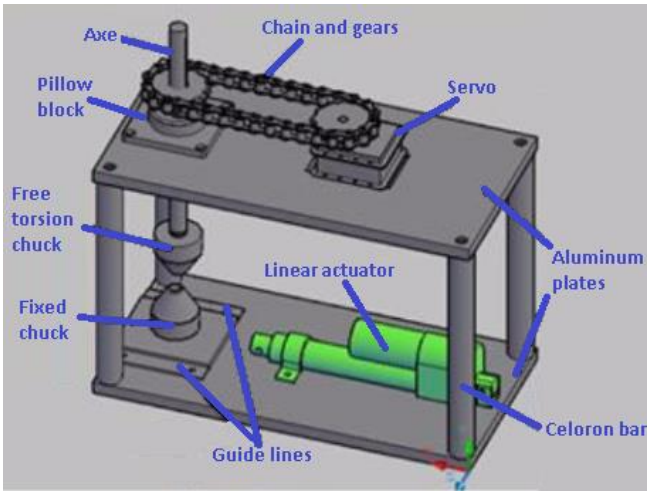

Fig. 6 Principal elements of the torsion fatigue machine.

Two important characteristics of this machine are: its capacity to record the number of cycles of fatigue life in real time and to stop the counter of cycles automatically when fracture occurs. The last capacity was implemented through

current continuity along the testing specimen: when fracture occurs, current continuity is interrupted and both devices turn off (the torsion machine and the electronic counter). In the case of non-conducting material such as polymers, current continuity is provided by a thin conductor wire which is broken simultaneously with the specimen failure.

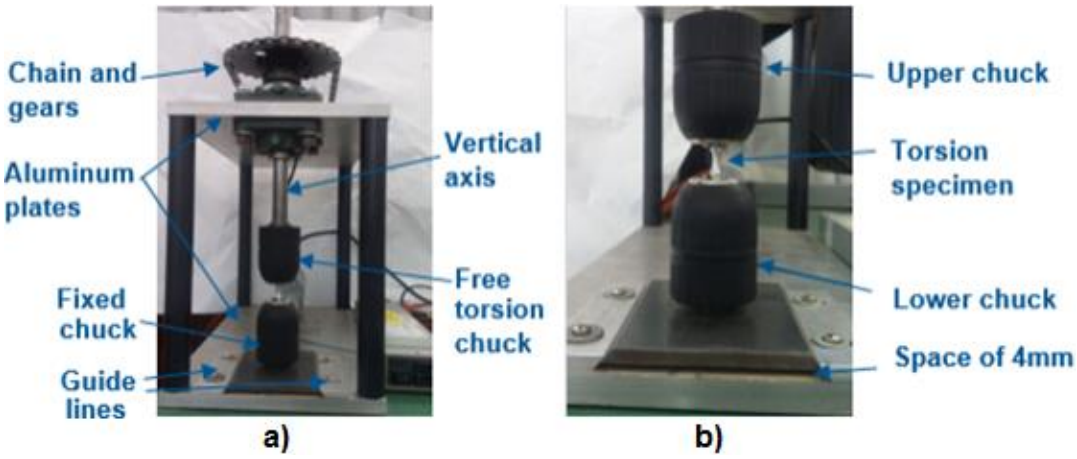

Fig. 7 a) Frontal view of the torsion fatigue machine, b) Amplification for chucks and testing specimen.

5. Results and discussion.

5.1. Torsion fatigue results.

Torsion fatigue tests were performed and analyzed by optical microscope and SEM on two aluminum alloys: 6061-T6 and 6063-T5. The tests were obtained at room temperature (22°C) and with environmental humidity comprised between 35% and 45%. The two aluminum alloys were subjected to torsion fatigue tests at four levels of applied load, induced by a fixed torsion angle of: 2.43°, 2.16°, 1.89°, 1.62°, which corresponds to 50.9%, 45.2%, 39.6%, 34% the shear strength of 6061-T6 alloy and 90%, 80%, 70%, 60% of 6063-T5 aluminum alloy, Fig. 8. All tests were performed at 10 Hz of frequency and with the loading ratio R=0. The lines in Fig. 8 have been obtained by logarithmic interpolation of the experimental data.

The torsion fatigue behavior plotted in Fig. 8 suggests that for the high applied load (high torsion angle), the aluminum alloy 6061-T6 presents higher torsion fatigue endurance compared to the 6063-T5; this difference seems to decrease with decreasing the applied load.

The Figs. 9a and 9b show laterals views of torsion fracture where predominant ductile behavior was observed on the aluminum alloy 6063-T5: this fracture is characterized by a crack path almost perpendicular with respect to the longitudinal axis of the testing specimen. On the other hand, a predominantly brittle

fracture is observed in the neck section of aluminum alloy 6061-T6, as illustrated on Fig. 9c: in this figure appears the lateral fracture path near to 45° in regard the longitudinal axis of specimen. Furthermore, a frontal fracture surface of another 6061-T6 specimen is shown on Fig. 9d, presenting important plastic deformation at the external zone of fracture surface (dark zones), where the cracks initiate. In the last fracture surface is localized also a granular zone at the center (bright zone), related to a rapid crack propagation with no high apparent plastic deformation.

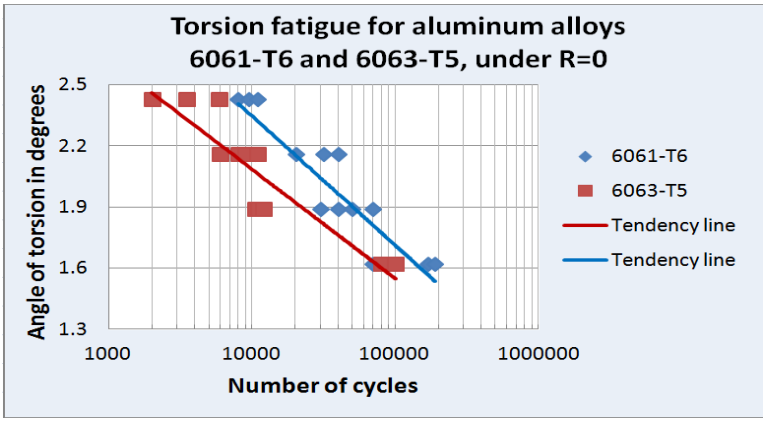

Fig. 8 Torsion fatigue endurance for the aluminum alloys: 6061-T6 and 6063-T5, under load ratio R=0.

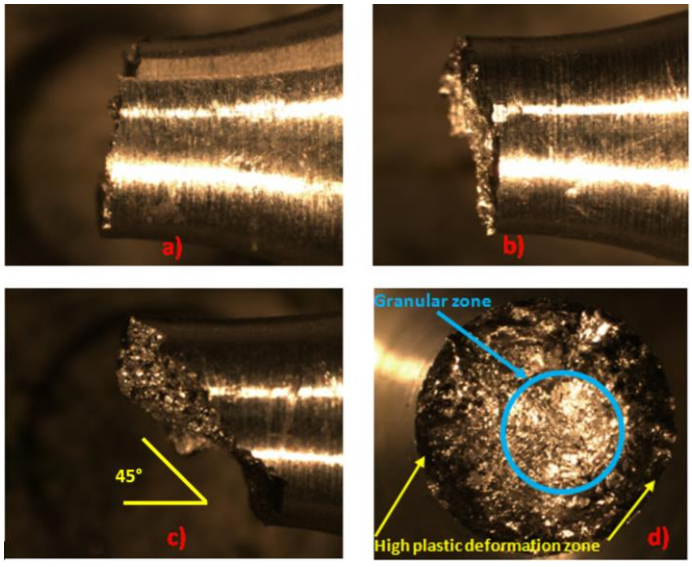

Fig. 9. Torsion fracture paths: a) and b) lateral ductile fracture for aluminum alloy 6063-T5; c) lateral brittle fracture and d) frontal fracture surface for aluminum alloy 6061-T6.

Images by SEM (scanning electron microscope), show that microcracks initiate at the specimen surface and propagate on a radial path towards its center for the aluminum alloys 6061-T6, as shown on Fig. 10a. Such microcracks are the result of the coalescence of microvoids at microscopic scale which are associated to plastic deformation at this scale, as illustrated in Fig. 14b.

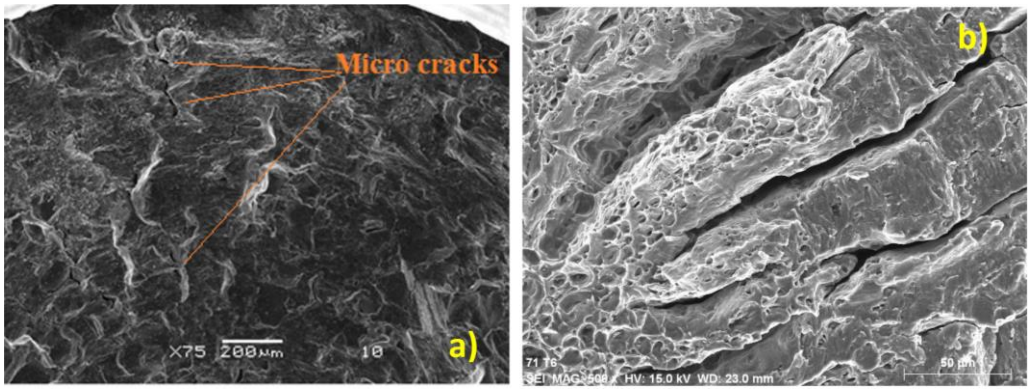

Fig. 10. Fracture surfaces of 6061-T6 aluminum alloy observed by scanning electron microscope: a) 200 μm of amplification, b) 50 μm of amplification.

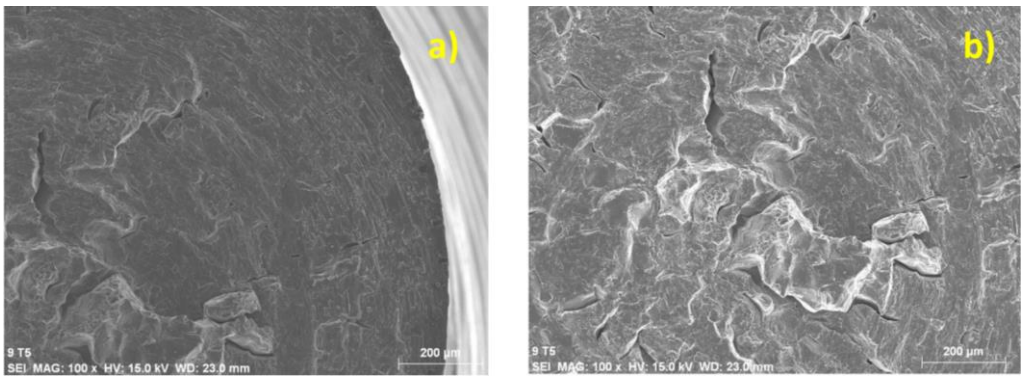

Fig. 11. Fracture surfaces of 6063-T5 aluminum alloy observed by scanning electron microscope: a) micrograph at one corner of fracture surface, b) micrograph at the center of fracture surface

Concerning scanning electron microscope images for fracture surfaces under torsion testing on aluminum alloy 6063-T5, in Fig. 11a and 11b are presented the principal features: plastic deformation and microcracks are observed in radial direction as in the previous case with the hardening effect at the microscopic scale [24, 25]; nevertheless, this time the density of microcracks in radial direction seems to decrease, Fig. 11a: a higher ductility of aluminum alloy 6063-T5 compared to

6061-T6, tends to reduce the crack initiation sites. On the other hand, at the center of fracture surface of this aluminum alloy are observed radial microcracks generated by large microvoids, Fig. 11b. The increase of ductility on aluminum alloys induces an increase of the sizes of microvoids, leading to facilitate the coalescence of them and reducing the crack propagation paths, when subjected to fatigue load [26].

6. Conclusions

The following conclusions can be draw from this work:

1. The description of a new torsion fatigue machine is presented with experimental results on the AISI aluminum alloys: 6061-T6 and 6063-T6.
2. The precision of the torsion applied angle with this torsion machine is close to 0.1 degrees.
3. Numerical simulations indicate high shear elastic strain along the variable radius section: the higher value is located at the surface and in the necking section of the specimen.
4. It was obtained the elastic energy accumulated in the torsion testing specimen in function of the applied torque and the torsion angle: the case for aluminum alloy 6061-T6 and the general expression.
5. The induced torsion angle θ increases dramatically with the reduction of the neck section radius of specimen (parameter a); whereas the reduction on parameter b induces a moderate increase on the torsion angle. The torsion angle θ increases with the geometrical dimension c, from 0 to an asymptotical value.
6. From the torsion fatigue results, the aluminum alloy 6061-T6 presents higher torsion fatigue endurance compared to the 6063-T5 for the high applied load (high torsion angle); this difference seems to decrease with decreasing the applied load.
7. The fracture surfaces show radial propagation of microcracks for the two aluminum alloys. The higher ductility of aluminum alloy 6063-T5 compared to 6061-T6 induces higher sizes of microvoids on the first alloy, leading to reduce the crack initiation sites and increasing microcrack size.

Acknowledgments

The authors gratefully acknowledge the University of Michoacan (UMSNH) in Mexico for the facilities provided in developing this work. A special mention of gratitude to CONACYT (The National Council for Science and Technology, Mexico) for the financial support to this work by the grant: CB-241117-2014.

R E F E R E N C E S

[1] *D. Chandra, J. Purbolaksono, Y. Nukman, H.L. Liew, S. Ramesh, M. Hamd*, "Fatigue crack growth of a corner crack in a square prismatic bar under combined cyclic torsion–tension loading", International Journal of Fatigue, vol. 64, 2014, pp. 67-73.

[2] *X. Wang, M. Chen,, G. Pu, and Ch.. Wang*, "Residual fatigue strength of 48MnV crankshaft based on safety factor", Journal of Central South University of Technology, vol. 12, no. 2, 2005, pp. 145-147.

[3] *J.W Hur*, "An experimental study on fatigue safety life assessment of aircraft engine support structure", International Journal of Precision Engineering and Manufacturing, vol. 12, no. 5, 2011, pp. 843-848.

[4] *P.R. Raju, B. Satyanarayana, K. Ramji, and K.S. Babu*, "Evaluation of fatigue life of aluminum alloy wheels under radial loads", Engineering Failure Analysis., vol. 14, no. 7, 2007, pp. 791-800.

[5] *Z.L. Wang, H. Xiao*, "A study of metal fatigue failure as inherent features of elastoplastic constitutive equations", Advanced Structured Materials, vol. 64, 2015, pp. 529-540.

[6] D.D. Cioclov, 2009, "Fatigue failure risk assessment in load carrying components", Security and reliability of damaged structures and defective materials, Eds Pluvinage, G. and Sedmak, A., 2009, pp. 25-73. Springer, New York – Berlin.

[7] *Y. Liu, and S. Mahadevan*, "A unified multiaxial fatigue damage model for isotropic and anisotropic materials", International Journal of Fatigue, vol. 29, no. 2, 2007, pp. 347-359.

[8] *J. Papuga*, "A survey on evaluating the fatigue limit under multiaxial loading", International Journal of Fatigue, vol. 33, no. 2, 2011, pp. 153-165.

[9] *L. Susmel*, "A unifying approach to estimate the high-cycle fatigue strength of notched components subjected to both uniaxial and multiaxial cyclic loadings", Fatigue & Fracture of Engineering Materials & Structures, vol. 27, no. 5, 2004, pp. 391-411.

[10] *F.M. Peña Bustos, C.A. Alvarez Vargas*, "Design and construction of a torsional fatigue testing machine operated by inertial loads", DYNA, vol. 79, no.172, 2012, pp. 46-55.

[11] *D.I. Fletcher and J.H. Beynon*, "Development of a machine for closely controlled rolling contact fatigue and wear testing", Journal of Testing and Evaluation, vol. 28, no. 4, 2000, pp. 267-275.

[12] *M. Feng and M. Li*, "Development of a computerized electrodynamic resonant fatigue test machine and its applications to automotive components", (No. 2003-01-0951). SAE Technical Paper, 2003.

[13] *Anon*, "Wöhler's experiments on the fatigue of metals", Engineering (London), vol. 11, 1871, pp. 199-200, 221, 244-245, 261, 299-300, 326-327, 349-350, 397, 439-441.

[14] *J.W. Clark and R.L. Moore*, "Torsion test of aluminum-alloy stiffened circular cylinders", NACA Reports, Technical Note 2821, 1952.

[15] *H. Hussain*, "Torsion fatigue system for mechanical characterization of materials," Doctoral dissertation, Ohio University, 2000.

[16] *F.T. Joaquim, R. Barbieri and N. Barbieri*, "Investigating torsional fatigue with a novel resonant testing fixture", International Journal of Fatigue, vol. 31, no. 8-9, 2009, pp. 1271-1277.

[17] *J.L. Avila Ambriz, G.M. Dominguez Almaraz,, E. Correa Gómez and J.C. Verduzco Juárez*, "Torsion fatigue endurance and load ratio confrontation R=0 VS. R=-1 on the AISI 6061-T6 aluminum alloy," International Journal of Advanced Research, vol. 3, no. 12, 2015, pp. 1428-1433.

[18] *C.M. Hyun, S. Salleh, N. Ahmad, A. Ourdjini, E. Hamzah*, "Influence of carbon content on the mechanical properties of ultra-high strength of coated steel wire", Jurnal Teknologi, vol. 69, no. 1, 2014, pp. 89-95.

[19] *M. Murashkin, I. Sabirov, D. Prosvirnin, I. Ovid'ko, V. Terentiev, R. Valiev, S. Dobatkin*, "Fatigue behavior of an ultrafine-grained Al-Mg-Si alloy processed by high-pressure torsion", Metals, vol. 5, no. 2, 2015, pp. 578-590.

[20] *M. Marini, A.B. Ismail*, "Torsional deformation and fatigue behaviour of 6061 aluminium alloy," HUM Engineering Journal, vol. 12, no. 6, 2011, pp. 21-32.

[21] *H. Mayer*, "Ultrasonic torsion and tension–compression fatigue testing: Measuring principles and investigations on 2024-T351 aluminium alloy", International Journal of Fatigue, vol. 28, no. 11, 2006, pp. 1446–1455.

[22] *H. Mayer, R. Schuller, U. Karr, D. Irrasch, M. Fitzka, M. Hahn, M. Bacher-Höchst*, "Cyclic torsion very high cycle fatigue of VDSiCr spring steel at different load ratios", International Journal of Fatigue, vol. 70, 2015, pp. 322–327.

[23] *J.L. Avila Ambriz, G.M. Domínguez, Almaraz, E. Correa, Gómez and R. González Bernal*, "Fatigue testing machine for developing fatigue tests under different modes, including: rotating bending, torsion and its combinations," Journal of Mechatronics, vol. 2, no. 4, 2014, pp. 246-250.

[24] *V. Tvergaard, J.W. Hutchinson*, "Two mechanisms of ductile fracture: void by void growth versus
multiple void interaction", International Journal of Solids and Structures, vol. 39, no. 13-14, 2002, pp. 3581-3597.

[25] *Y. Estrin, A. Vinogradov*, "Fatigue behaviour of light alloys with ultrafine grain structure produced by severe plastic deformation: An overview", International Journal of Fatigue, vol. 32, 2010, pp. 898-907.

[26] *A.A. Benzerga*, "Micromechanics of coalescence in ductile fracture", Journal of the Mechanics and Physics of Solids, vol. 50, no. 6, 2002, pp. 1331-1362.